Impact of CB1 Receptor Deletion on Visual Responses and Organization of Primary Visual Cortex in Adult Mice

Reza Abbas Farishta,[1] Céline Robert,[1] Olivier Turcot,[1] Sébastien Thomas,[1] Matthieu P. Vanni,[1] Jean-François Bouchard,[2] and Christian Casanova[1]

[1]Laboratoire des Neurosciences de la Vision, École d'optométrie, Université de Montréal, Montréal, Québec, Canada
[2]Laboratoire de Neuropharmacologie, École d'optométrie, Université de Montréal, Québec, Canada

Correspondence: Christian Casanova, School of Optometry, Université de Montréal 3744 Jean-Brillant, Room 260-7, Montréal, QC H3T 1P1, Canada;
christian.casanova@umontreal.ca.

Submitted: July 13, 2015
Accepted: October 25, 2015

Citation: Abbas Farishta R, Robert C, Turcot O, et al. Impact of CB1 receptor deletion on visual responses and organization of primary visual cortex in adult mice. *Invest Ophthalmol Vis Sci*. 2015;56:7697–7707. DOI:10.1167/iovs.15-17690

Purpose. The endocannabinoids (eCBs) and their receptors are expressed in the cortex of developing animals where they act as a neuromodulating system during critical stages of brain development such as cell proliferation and migration, and axon guidance. Little is known on the impact of the cannabinoid system on cortical map formation and receptive field properties of cortical sensory neurons. The present study evaluates in vivo the functional organization of the primary visual cortex (V1) of mice lacking cannabinoid CB1R receptor ($cnr1^{-/-}$).

Methods. Using optical imaging of intrinsic signals, azimuth, and elevation maps of $cnr1^{-/-}$ mice were compared with their wild-type littermates ($cnr1^{+/+}$).

Results. Topographic maps were affected in mutant mice as they exhibited narrower visual field and changes in the shape of V1. CB1R exerted its action in an axis dependent manner as all changes were observed in the azimuth axis. Spatial frequency and contrast sensitivity were also compared between the two groups. Both properties were affected by the chronic lacking of CB1R as mutant mice exhibited a significantly lower contrast sensitivity as well as lower spatial frequency selectivity.

Conclusions. Taken together, these results suggest an important role for CB1R in cortical map formation. Our results also clearly demonstrate the impact of CB1R in the development of visual properties of primary visual cortex neurons. Because psychoactive effects of cannabis consumption on visual experience are mediated mainly through CB1R, our results could possibly explain neuronal mechanisms involved in those perceptual changes.

Keywords: CB1, cannabinoid system, optical imaging, retinotopy, visual cortex, contrast modulation, mice

In the brain, neurons are organized in modality-specific areas where neighboring neurons share common properties. This is best illustrated in the visual system where neurons are distributed according to the spatial position of their receptive fields (RF) in the visual field.[1] This functional organization takes place during development through a combination of genetically-driven and activity-dependent mechanisms.[2,3] The establishment of cortical maps is regulated by signaling molecules carried by thalamocortical axons, and by membrane receptors expressed in the target areas.[4]

Numerous systems of axonal guidance and neuromodulation have been identified,[5] including the lately-discovered endocannabinoid system.[6] This system is composed of endogenous ligands known as endocannabinoids (eCBs), their respective synthesis and degradation enzymes and two principal receptors, CB1R and CB2R. The endocannabinoid system is known to participate in several stages of brain development such as cell proliferation and migration, and axon guidance.[7–13]

CB1Rs are highly expressed in many structures involved in the processing of visual information, such as the retina[14,15] superior colliculus (SC), lateral geniculate nucleus (LGN), and primary visual cortex (V1).[16] CB1R agonists and antagonists are known to modulate the guidance of retinal ganglion cell (RGC) axons and the morphology of their growth cones. Intravitreous injections of CB1R antagonists cause aberrant retinofugal projections in the SC and the LGN, indicative of their key role in the development of the visual system.[12]

Despite numerous studies showing that eCBs can disrupt projection patterns of retinofugal fibers in the thalamus and the midbrain during development, their role in the establishment of visual topographic cortical map formation has not been investigated. Moreover, most of these studies were conducted in the context of developmental processes, and therefore, did not provide information on the role of eCBs in visual information processing in the adult brain. Because eCBs are virtually present everywhere from the retina to the visual cortex, their involvement in modulation of visual information is very likely.

In this study, we evaluated the functional role of CB1R in the visual cortex using mice lacking *cnr1* ($cnr1^{-/-}$), the gene coding for CB1R, using optical imaging of intrinsic signals (IOS).[17] The spatial organization of retinotopic cortical maps was characterized and compared between $cnr1^{-/-}$ and wild-type mice to determine the impact of *cnr1* deletion on thalamocortical connectivity. We also investigated the impact of CB1R on visual responses of cortical neurons, examining contrast sensitivity and spatial frequency selectivity.

Results indicate that retinotopic cortical maps were altered in *cnr1*$^{-/-}$ mice compared with their *cnr1*$^{+/+}$ littermates, especially along the azimuth axis. *Cnr1*$^{-/-}$ mice exhibited a smaller visual field as well as differences in V1 shape. Moreover, contrast sensitivity and spatial frequency selectivity were significantly reduced in *cnr1*$^{-/-}$ mice when compared with the *cnr1*$^{+/+}$ controls.

Materials and Methods

Animal Preparation

All procedures were carried out in accordance with the guidelines of the Canadian Council for the Protection of Animals and the ARVO Statement for the Use of Animals in Ophthalmic and Vision Research, and were approved by the Ethics Committee on animal research of the Université de Montréal (Montréal, Québec, Canada). A total of 34 adult animals were used in this study (21 *cnr1*$^{-/-}$ and 13 *cnr1*$^{+/+}$) out of which 22 (15 *cnr1*$^{-/-}$ and 7 *cnr1*$^{+/+}$) were imaged for both retinotopic organization and functional properties of V1 (contrast and spatial frequency selectivity) neurons while the 12 remaining animals were imaged to measure the functional properties only (6 *cnr1*$^{-/-}$ and 6 *cnr1*$^{+/+}$). The *cnr1* transgenic mice were obtained from Beat Lutz (Institute of Physiological Chemistry and Pathobiochemistry, University of Mainz, Germany) and were on a C57BL/6N genetic background. Transgenic mice were compared with background and age-matched *cnr1*$^{+/+}$ controls from separate colonies. Mice were anesthetized with urethane (1.5 g/kg, intraperitoneal [i.p.]) complemented by atropine (0.05 mg/kg, subcutaneous [s.c.]). Lidocaine (2%) was injected locally to all incision sites. A tracheotomy was performed, and the animals were placed in a stereotaxic frame and supplied with airflow of saturated O_2. Body temperature was maintained at 37°C through a feedback-controlled heat pad. Electrocardiogram was continuously monitored to evaluate the depth of anesthesia and the animal welfare. The mouse cortex was imaged through the skull after scalp incision over the visual cortex (Fig. 1A). Imaging chambers were glued on the skull, filled with agarose (1%), and sealed with a glass coverslip. Eyes were hydrated regularly to avoid formation of cataracts and to preserve acuity.[18] At the end of each experiment, the animal was euthanized by an overdose of pentobarbital sodium (Euthanyl, 0.1 mL, i.p.; Bimeda-MTC, Ontario, Canada). Post hoc PCR analysis was performed on each animal to confirm the genotype.

Visual Stimulation

Visual stimuli were generated using a custom-made software and presented on a screen placed 20 cm in front of the mouse eyes using a liquid crystal display (LCD) projector (150° × 135° of visual angle). To acquire and characterize V1 maps, a continuous stimulation paradigm was used[19] where white bars (150 cd/mm^2, 2° wide) were periodically moving at 0.2 Hz horizontally or vertically over a black background in order to generate elevation and azimuth maps, respectively. In a subset of experiment, monocular stimulation was used in order to estimate the size of binocular visual cortex by measuring the ipsilateral cortical surface. To examine the functional properties of V1 neurons, namely sensitivity to contrast and selectivity to spatial frequency, full-field sine wave drifting gratings (four directions: 0°, 90°, 180°, 270°) were presented in a randomized fashion for 2 seconds and spaced by a blank presentation lasting 18 seconds intervals (gray background only, 75 cd/mm^2). For contrast sensitivity, five different contrast values were used: 6%, 12%, 25%, 50%, and 100% presented at 0.02 cyc/deg at a temporal frequency of 3 Hz. For spatial frequency selectivity, four distinct frequencies were used: 0.005, 0.01, 0.02, and 0.04 cyc/deg, presented at 100% contrast.

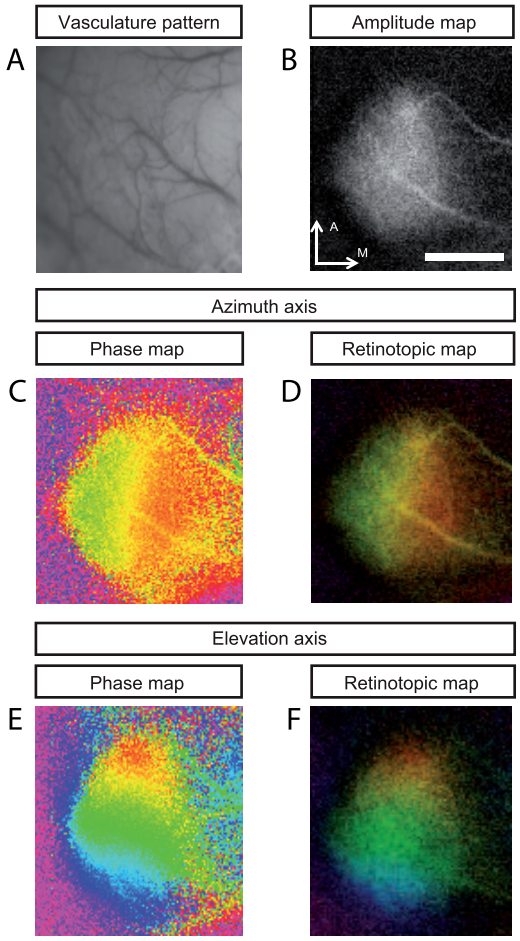

Figure 1. Imaging cortical retinotopy in *cnr1*$^{+/+}$ mice. (**A**) Vasculature pattern centered on primary visual cortical area. (**B**) Grayscale coded response amplitude maps. (**C**) Phase maps (*left*) and retinotopic maps (*right*) in response to a 2° moving bar drifting along the azimuth axis. (**D**) Phase maps (*left*) and retinotopic maps (*right*) in response to a 2° bar drifting along the elevation axis.

Data Acquisition and Analysis

The skull was first illuminated with a 545 ± 20 nm light to adjust the focus and obtain an anatomical reference image (Fig. 1A). The acquisition of intrinsic signals was performed using a 630 ± 30 nm light.[20] Images were captured with a 12 bits charged-coupled device (CCD) camera (1M60; Dalsa, Colorado Springs, CO, USA) driven by the Imager 3001 system (Optical Imaging Ltd., Rehovot, Israel) and fitted with a macroscopic lens (AF Micro Nikkor, 60 mm, 1:2.8D; Nikon Canada, Mississauga, ON, Canada), which provided a greater depth of field and working distance. Spatial resolution of images was 28 μm/pixel. For retinotopic mapping, 2400 frames were collected during 10 minutes. When stimulating episodically, 80 frames were captured for 20 seconds for every contrast and spatial frequency tested.

Data were analyzed using scripts running with MATLAB (Version 2009b; MathWorks, Natick, MA, USA).

Light Fluctuation Correction

Because of the relatively small size of optical responses, every fluctuation in the light source or large global activity fluctuations can significantly alter the signal to noise ratio. In order to resolve this issue, an illumination correction method based on average activity removal was applied on the data.[21,22] Raw data were corrected for each pixel (*i,j*) with

$$R_{c_{i,j,f}} = \frac{\left(R_{i,j,f} - \left[S_{i,j} \times \frac{T_f}{\bar{R}}\right]\right)}{S_{i,j}}, \quad (1)$$

where $R_{i,j,f}$ and $R_{c_{i,j,f}}$ are the raw and corrected data. T_f is the light time course, defined as:

$$T_f = \frac{1}{XY}\sum_{i=x}^{x+X}\sum_{j=y}^{y+Y} R_{i,j,f}, \quad (2)$$

where x, y, X, and Y are the position and the size of the region of interest used as a noise reference. $S_{i,j}$ is the map of light average, defined as:

$$S_{i,j} = \frac{1}{F}\sum_{f=1}^{F} R_{i,j,f}, \quad (3)$$

and $\bar{R}$ is the light average defined as:

$$\bar{R} = \frac{1}{F}\sum_{f=1}^{F} T_f, \quad (4)$$

where F is the number of frames. The reference region was chosen as a zone with no visual activation, low vascular noise (e.g., no blood vessel) and a high level of illumination. Then this signal was decomposed by Fourier transform to obtain phase and magnitude matrixes ($\varphi_{i,j,n}$, and $A_{i,j,n}$, Figs. 1C, 1E) as described in the paradigm of Kalatsky and Stryker.[19]

Functional Cortical Maps

While the phase values at the stimulus frequency were used to determine retinotopy maps,[19] an improved representation of retinotopy can be obtained by normalizing the phase by the signal amplitude (Figs. 1D, 1F). The resulting maps were used to delimit the borders of the regions of interest (ROI) corresponding to the visual cortex. Several attempts to implement automatic delimitation of ROI were performed but none of them provided consistent results and often introduced errors. Therefore, we performed a manual delimitation of the ROI. To avoid potential bias, we split data in two halves, each one attributed to one coauthor. Next, data samples were randomly picked and the two selected coauthors were asked to draw ROIs, without any clue of the genotype associated with the samples. Finally, we performed statistical tests that indicated that no interauthor bias existed, and that quantifications were robust ($P > 0.05$ for every parameter measured between the two data set halves). For all mice, responses from both cortices were averaged.

An ovality index, corresponding to the ratio between the height and width of the ROI, was used as a shape parameter of the visual cortex. The ratio of phases present in the retinotopic maps over the phases displayed was used as an estimate of the visual field represented in V1 (e.g., apparent visual field). The binocular visual fields were calculated using the proportion of phase values present in both hemispheres while the size the binocular cortex was estimated by measuring the ipsilateral cortical surface after monocular stimulation. A scatter index, calculated using the average difference between the phase value of each pixel with its surrounding pixel was used in order to quantify the smoothness in the visuotopic transitions within the visual cortex.[23,24]

Contrast Sensitivity and Spatial Frequency Selectivity

To evaluate contrast sensitivity and spatial frequency selectivity, each stimulus condition was presented 7 to 10 times, and responses were averaged across trials and directions associated with the variable tested. For each spatial frequency and contrast values/conditions, the response maps were calculated by measuring the absolute maximum difference of luminance before and after the presentation of the grating. Contrast response profiles were fitted to a sigmoid curve using a Naka Rushton function. A C_{50} value (contrast evoking half of the maximum response) was fitted for both groups. To determine the optimal spatial frequency, the spatial frequency evoking the strongest response was measured, on a pixel-by-pixel basis and averaged.

Statistical Analysis

For all analysis performed on visuotopic maps, *cnr1*$^{-/-}$ and *cnr1*$^{+/+}$ were compared using Student's *t*-test. Contrast sensitivity was compared using a Student's *t*-test on the average C_{50} value of both groups. Error bars depict standard deviation. An *F*-test was performed on spatial frequency selectivity distributions. Statistical analyses were performed using SPSS 17.0 (SPSS, Inc., Chicago, IL, USA) or Matlab.

Results

V1 Anatomo-Functional Properties

Visual stimulation by moving bars produced a robust activation in the visual cortex where retinotopic maps of V1 could be acquired. The following analysis is based on data originating from 15 *cnr1*$^{-/-}$ and 7 *cnr1*$^{+/+}$ mice.

Magnitude of Cortical Responses. We first compared the average magnitude of cortical responses between the two strains of mice in order to determine the impact of *cnr1* deletion on the strength of visually evoked intrinsic signals. Examples of magnitude maps are shown in Figure 1B where clear and well-defined activation areas were seen in the visual cortex of a *cnr1*$^{+/+}$ mouse after visual stimulation of the entire visual field. Signal amplitude was quantified as percentage of changes in optical reflectance. Figure 2A illustrates comparison of the signal magnitude between the two groups; no differences were seen in azimuth and elevation maps ($P > 0.20$ Student's *t*-test) suggesting that *cnr1* deletion does not affect the overall responsiveness of the visual cortex. The amplitudes of activation were (0.009% ± 0.0035) in *cnr1*$^{+/+}$ and (0.011% ± 0.0040) in *cnr1*$^{-/-}$ for the azimuth axis. For the elevation, magnitudes were (0.009% ± 0.002) in *cnr1*$^{+/+}$ and (0.010% ± 0.003) in *cnr1*$^{-/-}$.

Surface of Activation. Anatomical parameters, such as surface and shape of V1, were extracted from the analysis ROIs. Because CB1R is known to play a role in target selection of neurons at the subcortical level, we next quantified its effect on the organization of retinotopic cortical maps in V1. The V1 surface was computed by measuring the number of activated pixels in V1 of both strains and compared between the two strains (Fig. 2B). The average surface of activation was (3.287 mm^2 ± 0.184) for *cnr1*$^{+/+}$ and (3.126 ± 0.311 mm^2) for *cnr1*$^{-/-}$ along the azimuth, and (2.956 mm^2 ± 0.276) for *cnr1*$^{+/+}$ and

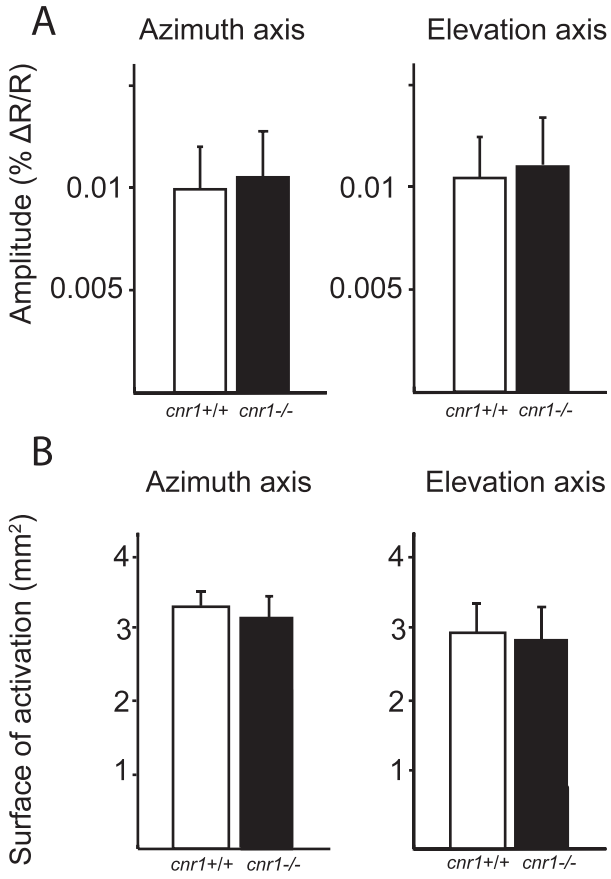

FIGURE 2. Comparison of amplitude and surface of activation elicited by visual stimulation. (**A**) Quantification of the amplitude of activation produced by visual stimulation. No differences were seen between the two groups for azimuth (*left*) and elevation (*right*) axis. (**B**) Quantification of the surface of activation elicited by visual stimulation. No differences were seen between the group for azimuth (*left*) and elevation (*right*).

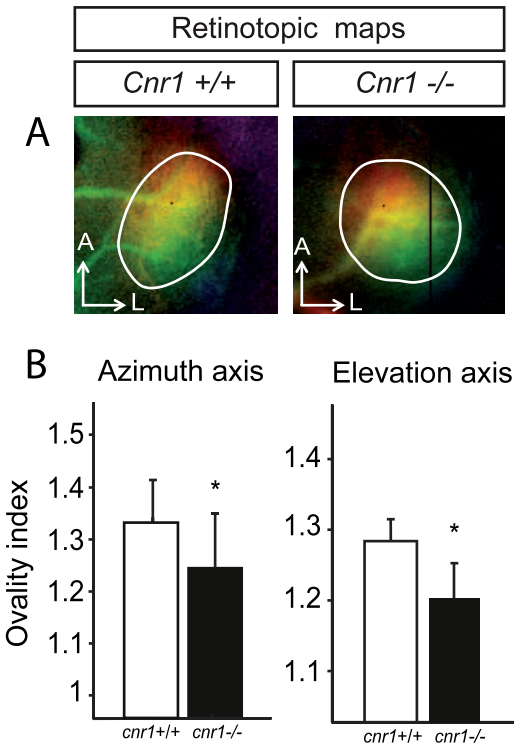

FIGURE 3. Primary visual cortex shape comparison between $cnr1^{+/+}$ and $cnr1^{-/-}$ mice. (**A**) Retinotopic maps used to quantify the ovality index for both $cnr1^{+/+}$ (*left*) and $cnr1^{-/-}$ mice (*right*). (**B**) Quantification of the ovality index used to compare shapes of V1 activated by drifting bars moving in the azimuth (*left*) and elevation axis (*right*). $cnr1^{-/-}$ mice (*black*) showed a rounder shaped V1 than $cnr1^{+/+}$ mice for both azimuth and elevation ($P < 0.01$, Student's *t*-test).

(2.870 mm^2 ± 0.354) for $cnr1^{-/-}$ along the elevation. Values were not statistically different ($P > 0.10$, Student's *t*-test).

After comparing multiple retinotopic activation maps of both strains, it was noted that V1 of $cnr1^{-/-}$ mice had a slightly different shape when compared with their $cnr1^{+/+}$ littermates. The shape of V1 was quantified by calculating an ovality index (i.e., length of the ROI divided by its width) of the visually activated cortex (Fig. 3A). Ovality indexes varied significantly for both the azimuth and the elevation as $cnr1^{-/-}$ mice had a smaller index (Fig. 3B), which resulted in a more 'rounded' shaped visual cortical area ($P < 0.01$, Student's *t*-test). Average indexes for azimuth were 1.334 ± 0.059 for $cnr1^{+/+}$ and 1.256 ± 0.056 for $cnr1^{-/-}$, and 1.279 ± 0.04 for $cnr1^{+/+}$ and 1.214 ± 0.057 for $cnr1^{-/-}$ along elevation.

Evaluation of the Retinotopic Organization of V1

Apparent Visual Field. The retinotopic organization of the visual cortex for both strains of mice was compared. Using the phase component of the signal acquired using a periodically drifting bar, it is possible to calculate the apparent visual field representation in the primary visual cortex. Consistent with previously reported visual field representation in mice,[19] gradients of phase values were seen in V1 along the elevation and azimuth axes of both $cnr1^{+/+}$ and $cnr1^{-/-}$ (Fig. 4). As expected in $cnr1^{+/+}$, the upper and lower visual fields were represented in the caudal and rostral regions (Fig. 4A). As for the azimuth axis, the central part of the visual field was represented at the lateral edges of V1, while the periphery was represented more medially (Fig. 4B).

Although this general retinotopic organization was preserved in $cnr1^{-/-}$ mice, the apparent visual field encoded in the visual cortex was significantly different. As exemplified in Figure 4B, $cnr1^{-/-}$ mice exhibited reduced visual field cortical representation when compared with $cnr1^{+/+}$ mice. $Cnr1^{-/-}$ mice had a significantly reduced visual field in the horizontal axis (Fig. 4C; $P < 0.0005$, Student's *t*-test) suggesting a role for CB1R in the establishment of visual field representation at the cortical level. For azimuth, average visual fields were 57.92° ± 2.24 and (50.78° ± 4.32) in $cnr1^{+/+}$ and $cnr1^{-/-}$ mice, respectively. Interestingly, no differences were found for the visual field representation along elevation, suggesting an axis-dependent role for CB1R in the development of these parameters.

Binocular Visual Field. The impact of *cnr1* deletion on binocular visual field was investigated in order to better identify the portion of visual field that showed differences between the two groups. Binocular visual field was quantified using maps elicited by a vertical bar moving along the azimuth (Fig. 5A). The binocular cortical region was defined by calculating the proportion of phase values existing in both hemispheres. Consistent with previous studies,[25] we found binocular cortices to be located at the lateral parts of V1 (Fig. 5A). To estimate the binocular visual field in both groups, we computed the ratio of binocular surface over the entire V1 surface. No significant differences were seen in both strains ($P > 0.1$) suggesting that visual field defects observed in $cnr1^{-/-}$

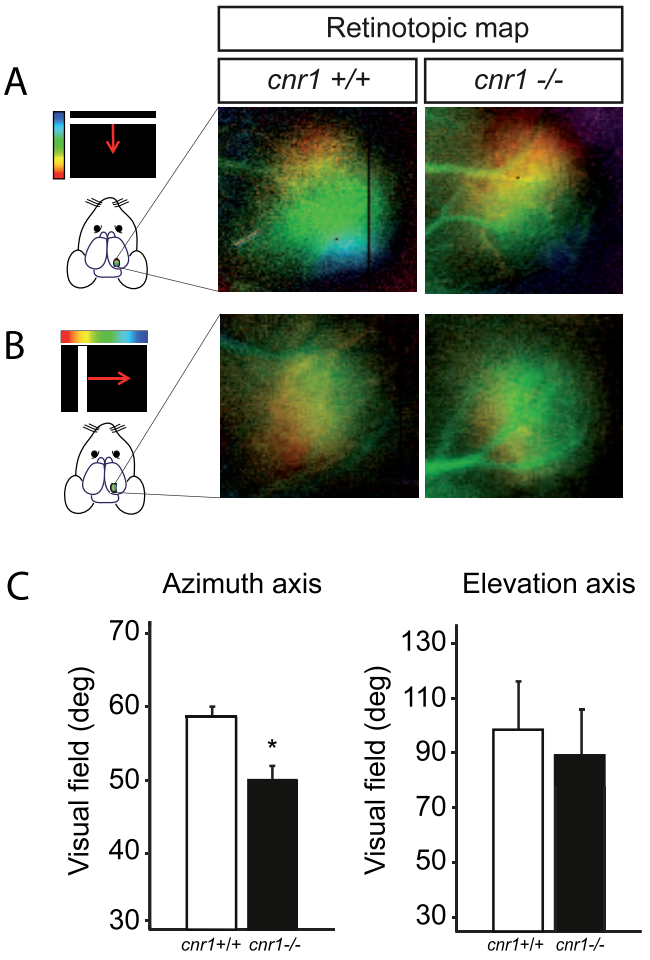

FIGURE 4. Apparent visual field comparison between $cnr1^{+/+}$ and $cnr1^{-/-}$ mice. (**A**) and (**B**) Schematic of the drifting bar moving along the elevation axis (**A**) and the azimuth axis (**B**) on the left. Phase maps resulting from visual stimulation for $cnr1^{+/+}$ and $cnr1^{-/-}$ mice on the *right*. (**C**) Quantification of the apparent visual field for both azimuth (*left*) and elevation (*right*) axis. $Cnr1^{-/-}$ mice showed a reduced visual field for the azimuth axis ($P < 0.001$, Student's *t*-test), while no significant differences were observed for the elevation axis ($P > 0.10$, Student's *t*-test).

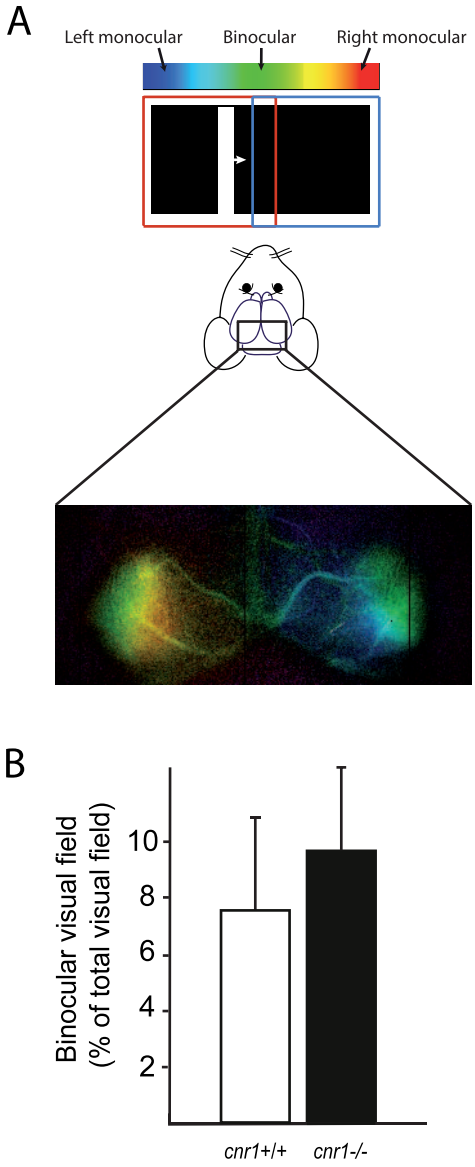

FIGURE 5. Binocular visual field comparison between $cnr1^{+/+}$ and $cnr1^{-/-}$ mice. (**A**) Schematic of the stimulation paradigm with a vertical bar moving periodically along the azimuth axis and activating corresponding zones in the visual cortex and an example of a retinotopic map generated by a bar moving in the azimuth axis. (**B**) Quantification of the binocular visual field calculated by the proportion of pixels in each hemisphere that showed similar phase of activation. No differences were observed between the two groups ($P > 0.10$, Student's *t*-test).

mice are not centrally located, but are more likely to come from a narrower peripheral visual field (Fig. 5B). Average binocular visual field represented 7.5% ± 2.28 for $cnr1^{+/+}$ and 9.9% ± 5.56 for $cnr1^{-/-}$ of the total visual field.

Ipsilateral Eye Cortical Map. The binocular cortex was also studied using vertically drifting bars presented under monocular conditions. This allowed us to measure the surface activated by projections coming from the ipsilateral eye, as they are restricted to the binocular part of V1[26–28] (Fig. 6A). No significant differences were observed ($P > 0.20$, Student's *t*-test) between groups (Fig. 6B). The average surface of ipsilateral cortical maps were 1.77 mm^2 ± 0.66 for $cnr1^{+/+}$ and 1.47 mm^2 ± 0.74 for $cnr1^{-/-}$.

Scatter Index. Because the cannabinoid system is known to play a role in the proper arrangement of visual projections during development,[12,13] we compared the progression of the receptive field positions along the retinotopic maps using a scatter index. Scatter indices were calculated using differences between phase values of individual pixels and those of their near neighbors. For maps with robust visual responses and well-organized receptive field transitions, these phase differences should be quite small due to the smooth progression of visual field representation in the visual cortex. Maps were more scattered in $cnr1^{+/+}$ than in $cnr1^{-/-}$ animals along the azimuth ($P < 0.02$, Student's *t*-test; Fig. 7). Scatter indices were (10.38° ± 3.19) for $cnr1^{+/+}$, and (7.93° ± 1.306) for $cnr1^{-/-}$ in the azimuth axis and (11.05° ± 3.05) for $cnr1^{+/+}$, and (10.58° ± 2.79) for $cnr1^{-/-}$ in the elevation axis. As found for the visual field representation (see above), difference in the scatter was noticeable along the azimuth only, strengthening the hypothesis of a greater role for CB1R in the horizontal coordinate system.

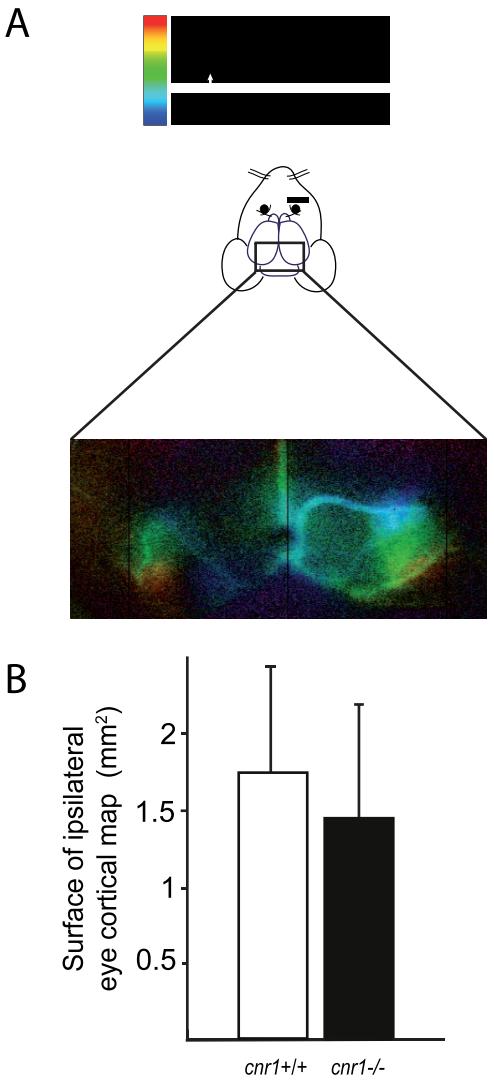

FIGURE 6. Binocular cortical surface comparison between *cnr1*$^{+/+}$ and *cnr1*$^{-/-}$ mice. (**A**) Schematic of the drifting bar moving along the elevation axis. Acquisitions were performed in monocular condition (left eye stimulated in this example) in order to stimulate the binocular visual cortex of the ipsilateraly stimulated eye located on the lateral edges of V1. (**B**) Quantification of the ipsilateral eye cortical map for both *cnr1*$^{+/+}$ and *cnr1*$^{-/-}$. No significant differences were observed in both groups ($P > 0.20$, Student's *t*-test). Average surface of ipsilateral cortical maps were 1.77 mm^2 ± 0.66 for *cnr1*$^{+/+}$ and 1.47 mm^2 ± 0.74 for *cnr1*$^{-/-}$.

Functional Properties of V1

Finally, we examined the effects of CB1 deletion on basic visual response characteristics such as spatial frequency selectivity and contrast sensitivity. The following data originates from 21 *cnr1*$^{-/-}$ and 13 *cnr1*$^{+/+}$ mice.

Spatial Frequency Selectivity. The impact of CB1 deletion on the spatial frequency selectivity of population of V1 neurons, was studied by comparing evoked responses to gratings of various spatial frequencies in both strains. Figure 8A shows examples of optical signal changes in response to spatial frequency values ranging from 0.005 to 0.04 cyc/deg in a *cnr1*$^{+/+}$ (left) and *cnr1*$^{-/-}$ (right) animal. In the *cnr1*$^{+/+}$ animal, all spatial frequencies generated robust activation in the visual cortex, with the maximum response obtained at 0.02 cyc/deg (red). Gratings of 0.01 cyc/deg (blue) also strongly activated

FIGURE 7. Quantification of scatter index for *cnr1*$^{+/+}$ and *cnr1*$^{-/-}$ mice for azimuth (*left*) and elevation (*right*). In the azimuth axis, *cnr1*$^{-/-}$ mice showed a lower scatter index compared with *cnr1*$^{+/+}$ mice ($P < 0.02$, Student's *t*-test) while no differences were seen in the elevation axis.

the cortex, although with a slightly lower amplitude. Gratings at lower (0.005 cyc/deg, in yellow) or higher (0.04 cyc/deg, in green) spatial frequencies produced weaker activation in the cortex suggesting a preferred spatial frequency between 0.01 and 0.02 cyc/deg. In the *cnr1*$^{-/-}$, a different pattern of activation was seen as the cortex was best activated by gratings of 0.01 cyc/deg followed by 0.005 and 0.02 cyc/deg, suggesting a shift of preference for lower spatial frequencies in these animals.

Figure 8B shows quantification of the preferred spatial frequency averaged across *cnr1*$^{+/+}$ (white bar) and *cnr1*$^{-/-}$ (black) animals. While visual cortices of *cnr1*$^{+/+}$ were best activated with gratings just below 0.02 cyc/deg (pixel-by-pixel average: 0.018 ± 0.0025), cortices of *cnr1*$^{-/-}$ mice showed a significantly reduced preferred spatial frequency (*t*-test, $P < 0.01$) as their primary visual cortex was more responsive for gratings close to 0.01 cyc/deg (0.012 ± 0.0022).

Figure 8C illustrates spatial frequency selectivity curves for both *cnr1*$^{+/+}$ and *cnr1*$^{-/-}$. As expected, the spatial frequency selectivity curve for *cnr1*$^{-/-}$ animals was clearly shifted toward lower spatial frequencies. While 0.02 cyc/deg produced the maximum response for *cnr1*$^{+/+}$, it generated just above 70% of the greatest response seen in *cnr1*$^{-/-}$. Moreover, while gratings of 0.04 cyc/deg were still able to produce significant responses in *cnr1*$^{+/+}$, they evoked less than 60% of the maximum amplitude in *cnr1*$^{-/-}$ mice. An *F*-test was performed on both distributions, revealing that the tuning profiles differed significantly between the two groups ($P < 0.02$). These results suggest that CB1R is involved in the mechanisms establishing spatial frequency selectivity at the cortical level.

Contrast Sensitivity. Additional imaging sessions were carried out to investigate the impact of CB1R on contrast sensitivity. Figure 9A illustrates averaged cortical responses in *cnr1*$^{+/+}$ (red) and *cnr1*$^{-/-}$ (black) mice as a function of contrast. There are clear differences between traces as *cnr1*$^{-/-}$ mice tended to exhibit a decreased sensitivity to contrast, especially at lower values. For instance, a 6% grating contrast elicited a significant response in *cnr1*$^{+/+}$ mice, but hardly produced any activation in *cnr1*$^{-/-}$ mice. Gratings of 12% contrast produced a slight change in optical responses in *cnr1*$^{-/-}$ mice but a strong activation in *cnr1*$^{+/+}$ animals. These differences in cortical responses tended to diminish for contrasts greater than 50%.

Data were fitted using a Naka Rushton function.[29,30] As shown in Figure 9B, contrast functions for *cnr1*$^{-/-}$ mice were shifted to the right when compared with *cnr1*$^{+/+}$ counterparts.

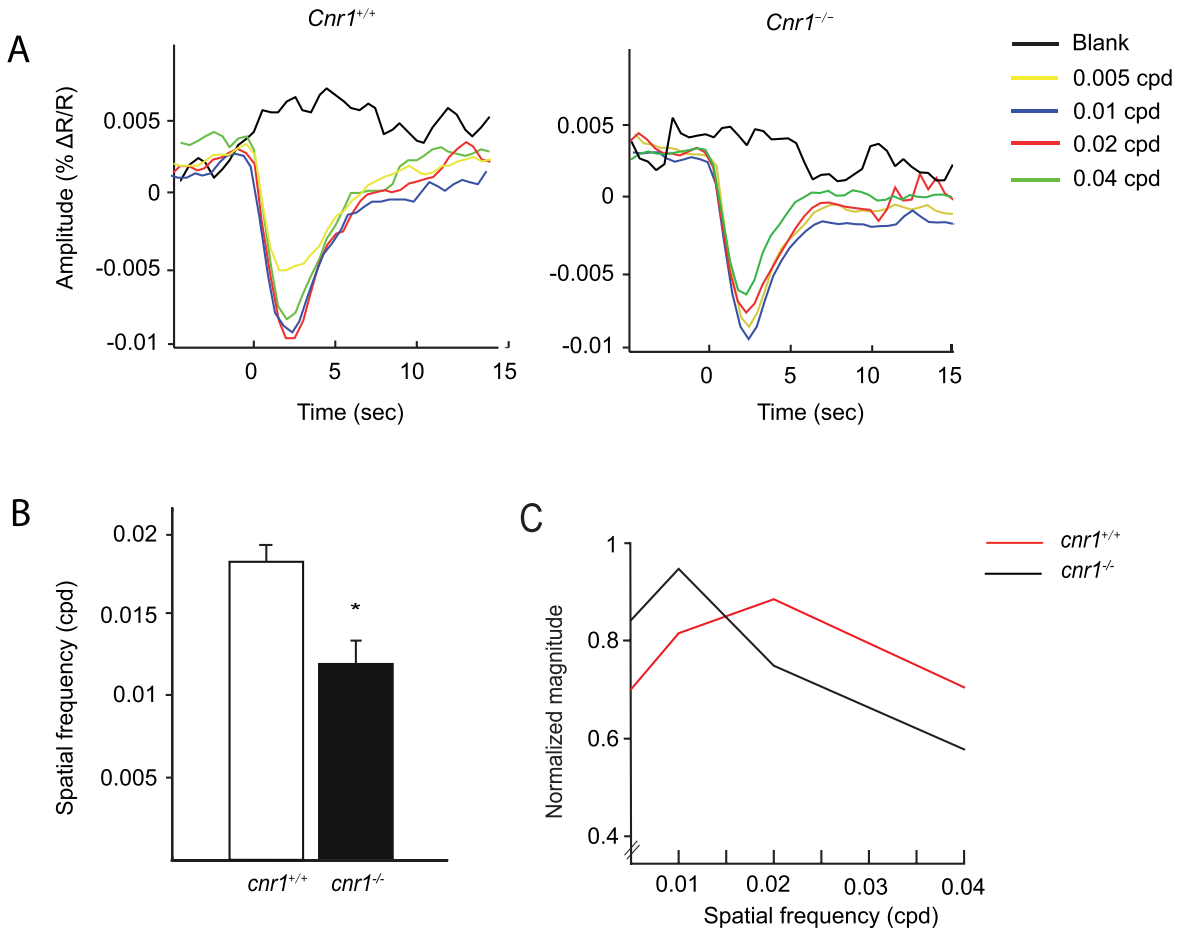

Figure 8. Optimal spatial frequencies of *cnr1*$^{+/+}$ and *cnr1*$^{-/-}$ mice. (**A**) Example of hemodynamic response function (HRF) traces to gratings of varying spatial frequencies. (**B**) Quantification of the optimal spatial frequency for both *cnr1*$^{+/+}$ and *cnr1*$^{-/-}$. The optimal spatial frequency was determined by the grating eliciting the maximum cortical response. *Cnr1*$^{-/-}$ mice showed a significantly reduced optimal spatial frequency ($P <$ 0.01 Student's *t*-test). (**C**) Spatial frequency selectivity curves for *cnr1*$^{+/+}$ (*red*) and *cnr1*$^{-/-}$ (*black*) differed significantly (*F*-test, $P < 0.02$).

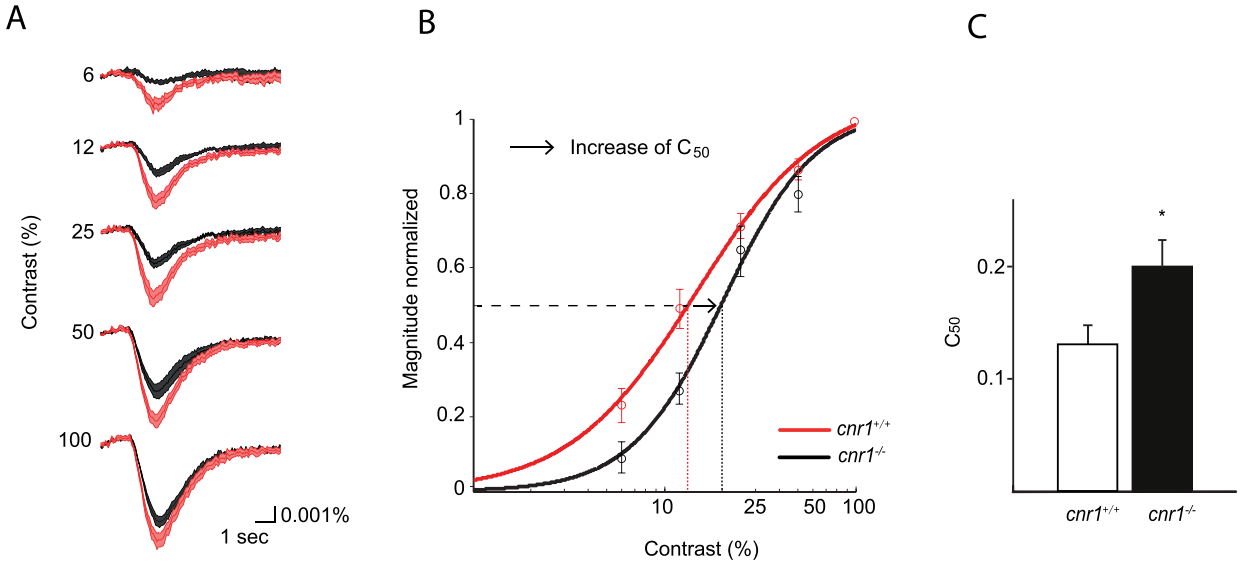

Figure 9. Primary visual cortex of *cnr1*$^{-/-}$ mice exhibits a decreased sensitivity to visual stimuli. (**A**) Averaged HRF recorded in *cnr1*$^{+/+}$ (*red*) and *cnr1*$^{-/-}$ (*black*) mice in response to gratings of different contrasts ranging from 6% to 100%. *Scale* indicates the percentage of change in light reflection captured by the camera as well as time. (**B**) Contrast sensitivity for *cnr1*$^{+/+}$ and *cnr1*$^{-/-}$ mice. Normalized amplitude of HRF (% of maximal response) in function of the luminance contrast of the stimulus. Data was fitted with a Naka-Rushton function. (**C**) Quantification of the C50 (contrast eliciting half of the maximum response) for *cnr1*$^{+/+}$ (*white*) and *cnr1*$^{-/-}$ (*black*). *Cnr1*$^{-/-}$ mice showed a significantly higher C50 when compared with *cnr1*$^{+/+}$ mice ($P < 0.0015$, Student's *t*-test).

Detailed analysis of the curves reveals that, in *cnr1*$^{-/-}$ mice, a higher contrast was needed to generate half of the maximum responses (C_{50}). Mean values of the C_{50} are presented in Figure 9C and show that *cnr1*$^{-/-}$ mice exhibited a significantly higher C_{50} than their *cnr1*$^{+/+}$ littermates (C_{50} for *cnr1*$^{+/+}$: 0.13% ± 0.04%, C_{50} for *cnr1*$^{-/-}$: 0.204% ± 0.03% [$P < 0.005$ Student's *t*-test]). These results suggest that CB1R is involved in the mechanisms subtending contrast sensitivity at the cortical level.

Discussion

To our knowledge, this study is the first to evaluate the role played by a key component of the cannabinoid system in the functional organization of the visual cortex. Our data presents clear evidence that *cnr1* deletion disturbs the structural and functional organization of the primary visual cortex as differences in shape and visual field representation were observed in *cnr1*$^{-/-}$ mice at adult age. In addition, the chronic deletion of *cnr1* affects the contrast sensitivity function and the spatial frequency selectivity, both considered to be critical for the establishment of visual perception.

The Influence of CB1R on the Functional Architecture of V1

When investigating the role of CB1R on cortical activity, robust retinotopic maps were obtained for both strains. However, the organization of their visual cortex was different, especially along the azimuth; V1 of *cnr1*$^{-/-}$ mice exhibited a narrower visual field representation, an altered shape of V1 and a significantly lower scatter index when compared with that of their *cnr1*$^{+/+}$ littermates.

CB1R Alters Cortical Maps in V1. Several research groups have used the visual system as a model to study the effect of a given receptor on target selection and cortical map formation. For example, deletions of receptors known to play a critical role in the establishment of geniculate-striate connections, such as Ephrin family, are known to significantly disturb V1 organization.[24,31] Our results suggest that CB1R plays a role in visual field establishment and/or maintenance at the cortical level as *cnr1*$^{-/-}$ mice exhibited a significantly reduced visual field representation, which was not accompanied by a shrinkage in the size of V1. Such changes have been reported before in other transgenic animals using either functional or behavioral assays. Mice lacking receptor Ten-m2 of the teneurin family were shown to exhibit defects in visual field, resulting from abnormal RGC projections to the LGN and SC.[32] Furthermore, this study reported a reduced number of RGCs projecting in the LGN of *cnr1*$^{-/-}$ mice, also leading to cortical visual field abnormalities. Similarly, we previously reported that CB1R plays a role in target selection as its pharmacologic activation leads to aberrant RGC projections in the LGN and SC.[12] Moreover, other studies have shown that CB1R plays a significant role in the survival of RGCs in rodents.[33] Thus, visual field defects in *cnr1*$^{-/-}$ mice are in line with the mechanisms insuring RGC survival and their proper projection patterns in the establishment of visual cortical maps involving the CB1R.

Another feature that significantly differed in *cnr1*$^{-/-}$ mice was the shape of its primary visual cortex. *Cnr1*$^{-/-}$ mice showed a more rounded V1 compared with the general oval-shaped V1 of *cnr1*$^{+/+}$ littermates. These results suggest a possible involvement of CB1R in processes that enable the patterning of the visual cortex. This patterning is usually attributed to transcription factors expressed in neocortical target areas, which determine the size and position of primary sensory cortices and regulate guidance information that governs the area-specific targeting of thalamo-cortical[7] axons.[34,35] Because *cnr1*$^{-/-}$ mice lacked CB1R in their entire visual system, one cannot precisely attribute effects observed to a given anatomical structure. However, it has been demonstrated that CB1R plays a role in the proper target selection of TC axons in the somatosensory system where TC axons of mice lacking CB1R were arranged in a less defined manner in area S1.[11] It is thus possible that a common mechanism is involved in the establishment of the precise patterning of visual cortical areas.

Another significant change observed while comparing retinotopic maps of both groups was the lower scatter index measured in *cnr1*$^{-/-}$ mice. Functionally, a lower scatter index suggests a more refined and orderly arranged succession of receptive field across the cortical surface. This result might seem contradictory to the general statement that CB1R deletion disrupts V1 retinotopic map development (reduced apparent visual field, altered shape of primary visual cortex). However, other studies have shown that impairments in a given characteristic of the visual cortex can significantly improve or enhance others. For example, after monocular deprivation, the shrinkage of ocular dominance domains is also accompanied by an enhanced distribution of orientation pinwheels.[36,37] Similarly, induced strabismus is known to sharpen boarders between ocular dominance columns.[38] Therefore, these studies indicate that compensatory rearrangement of the visual cortex can lead to supramaximal organization of some functional features.

Axis-Dependent Changes. Interestingly, most of the effects reported in the present study were observed along the azimuth axis. Other molecular systems have been shown to alter structural or functional aspects of the visual system in an axis-dependent manner.[24] For example, in mice lacking receptors of the ephrin family, functional maps in V1 along the azimuth axis are nearly abolished while those along elevation are maintained. The LGN of mice lacking β2 subunit of nicotinic acetylcholine receptor (*nAChR*-β2$^{-/-}$) does not exhibit a clear topographical organization in the azimuth axis while that along elevation is normal.[39] Behaviorally, these mice failed to track horizontally drifting gratings while they performed well for gratings moving vertically.[40] The effects of various molecular systems in the development of retinotopy in an axis-dependent manner have been shown not only in the cortex but also at the level of the retina and the SC.[31] Our data strengthen the view that different mechanisms regulate the formation of cortical maps in an axis dependent manner and indicate that CB1R is mainly involved in the establishment of a map along the azimuth.

Functional Properties of V1 Neuron Population

Changes in the architecture of the visual cortex described above were accompanied by modifications in the spatial properties of V1 neurons. Mutant mice showed a reduced spatial frequency selectivity and a weaker sensitivity for contrast compared with their *cnr1*$^{+/+}$ littermates, suggesting that the CB1R is involved in the fine-tuning of visual decoding properties of cortical neurons.

***Cnr1*$^{-/-}$ Mice Exhibit a Decreased Contrast Sensitivity.** Sensitivity to contrast is one of the most important attributes of the visual system as most visually responsive neurons are precisely tuned to respond to specific spatial–temporal variations of luminance contrast.[29] Along the central visual pathway, neurons from the retina to the LGN and the striate cortex show an increased firing in response to luminance contrast increment[41] suggesting that each structure plays a significant role in the establishment of contrast sensitivity and

contrast perception. Given the numerous structures that are involved in the processing of luminance contrast,[42] and the fact that all of them express CB1R, mechanisms associated with the change in cortical contrast sensitivity in *cnr1*$^{-/-}$ mice could very well originate from multiple sites. Although the rodent retina expresses CB1R receptor in all of its cells including photoreceptors (both cones and rods), bipolar cells, horizontal cells, and ganglion cells,[43] which are all known to play a critical role in the generation of contrast perception,[44] a recent study from our laboratory has reported no effects of CB1R receptors on retinal responses measured by ERG.[43] Electroretinographs recorded from *cnr1*$^{-/-}$ showed normal a- and b-wave in both photopic and scotopic conditions. While contrast selectivity per se was not tested, it is likely that retinal CB1R does not play a major role in the observed contrast changes. CB1R is widely expressed in the dLGN of rodents[12] and a recent study showed that local pharmacologic injections of CBs in this thalamic nucleus modulated spiking activity of geniculate neurons.[45] Because LGN cells can be modulated by the cannabinoid system independently from retinal and cortical processes, they may subtend, in part, the changes in contrast sensitivity observed in *cnr1*$^{-/-}$ mice.

Finally, the eCB system is highly likely to modulate visual processing at the cortical level. The primary visual cortex plays a key role in establishment of contrast perception. Simple neurons in V1 are known to exhibit a linear increase of their firing magnitude in response to logarithmic increments of grating contrast.[41] Moreover, the contrast sensitivity of V1 population neurons accurately predicts behaviorally measured contrast responses[46] further underlying the critical role of computations taking place in the striate cortex for contrast perception. Many studies have reported a modulatory effect of CB1R manipulation at the striate cortex level. For instance, eCB's can modulate deprivation-induced response depression in V1 neurons suggesting an involvement of CB1R in the ocular dominance shifts induced by sensory deprivation.[47] CB1R are also known to play a critical role in the maturation of GABAergic transmission in the visual cortex during development[48] and to modulate GABAergic mediated inhibition in the visual cortex at eye opening.[49] Moreover, it has been reported that the expression and localization pattern of CB1R is developmentally regulated[50] further indicating that CB1R plays an important role in physiological processes regulating critical period plasticity of V1 neurons. Thus, changes in cortical contrast selectivity in *cnr1*$^{-/-}$ mice could very well result from changes most likely occurring at the thalamic and cortical levels.

CB1R Effect on Spatial Frequency. The visual system of mammals is organized in parallel pathways, each one being preferably activated by visual stimuli with distinct spatial-temporal characteristics. For example, in primates, the cells of the parvocellular pathway exhibit a low temporal and high spatial frequency sensitivity while the cells of the magnocellular pathway are tuned for low spatial and high temporal frequencies.[51] This parallel organization was recently reported in the mouse visual system.[52] In this study, *cnr1*$^{-/-}$ mice exhibited a preference for lower spatial frequency and a reduced spatial frequency selectivity bandwidth. We hypothesize that the effects of *CB1R* deletion on spatial frequency in is likely mediated by changes in neurons exhibiting parvocellular-like RF.

Increasing the contrast of a stimulus is known to reduce the receptive field size of cortical neurons[53] and to increase spatial frequency bandwidth on most cortical neurons.[54] In our study, the *cnr1* deletion provokes changes in contrast and spatial frequency selectivity at the mesoscopic level, supporting the idea that these two properties share common physiological processes. However, because our technique provides data on the overall activity of a population of neurons, the exact contribution of CBR1 on receptive field properties at the single cell level or on specific cell types cannot be determined.

Links With Cannabis-Induced Changes in Visual Perception

Despite considerable research performed on the role of cannabinoids on visual function at the molecular and neuronal levels, very few studies have investigated the physiological processes by which cannabis consumption induce perceptual and behavioral changes. This is rather surprising since the effects of cannabis consumption on visual perception have been reported several times in first timers and chronic smokers. Case studies report several visual impairments including a distorted perception of distance, altered color vision, illusions of movement.[55] Several reports have also mentioned the effects of cannabis consumption on night vision.[56,57]

Because cannabinoids are the principal psychoactive components of Marijuana and hashish, and because their effects are known to be mainly mediated by CB1R,[58] our results may provide a physiological basis to understand the role played by this receptor in cannabis-induced visual distortions. However, even if some results of this study correlate with the visual symptoms accompanying cannabis usage in humans, cautious interpretation is commanded because we investigated the impact of life-long CB1R deletion on the visual function, whereas studies on the impact of cannabis consumption examined the effects of CB1R activation in a normal visual system.

One of the most important effects of CB1R deletion reported in this study is the shift of contrast sensitivity in knock-out mice suggesting a critical role for CB1R in the maintenance of this fundamental feature. Interestingly, the manipulation of CB1R in humans after cannabis consumption is known to better night vision,[57] a condition in which higher contrast sensitivity is often needed in order to compensate for low levels of light.[59]

Another key effect of CB1R deletion reported in this paper is the shift in selectivity toward lower spatial frequencies exhibited by knock-out mice. Similarly, cannabis consumption has been reported to decrease Snellen visual acuity scores in humans.[60] Because visual acuity and spatial frequency sensitivity both measure the spatial resolution of the visual system,[61] it is likely that a common CB1R-dependent mechanism modulates visual acuity in both species.

Conclusions

Results of this study show that the absence of CB1R has a functional impact on the visual cortex: Organization of V1 is altered along azimuth and contrast and spatial frequency selectivities are modified. Data presented here are in line with the important modulatory role attributed to the cannabinoid system in the development of visual pathways. This data further underlines the role played by the CB1R in visual processing because changes in visual perception reported after exogenous cannabis consumption[57] are mediated mainly through this receptor.[58]

Acknowledgments

Supported by Natural Sciences and Engineering Research Council of Canada (NSERC; Ottawa, ON, Canada), Canadian Institutes of Health Research (CIHR) (MOP-14825 Grants to CC and CIHR-130337 Grants to CC and J-FB; Ottawa, ON, Canada) and NSERC

Grants (J-FB; RGPAS 478115-2015 and RGPIN 2015-06582). Financial support from the School of Optometry and the Fonds de recherche du Québec-Santé (FRQ-S) Vision Research Network (RAF; Montreal, QC, Canada).

Disclosure: **R. Abbas Farishta**, None; **C. Robert**, None; **O. Turcot**, None; **S. Thomas**, None; **M.P. Vanni**, None; **J.-F. Bouchard**, None; **C. Casanova**, None

References

1. Holmes G. Disturbances of vision by cerebral lesions. *Br J Ophthalmol*. 1918;2:353–384.
2. Wiesel TN, Hubel DH. Single-cell responses in striate cortex of kittens deprived of vision in one eye. *J Neurophysiol*. 1963;26:1003–1017.
3. Crowley JC, Katz LC. Development of ocular dominance columns in the absence of retinal input. *Nat Neurosci*. 1999;2:1125–1130.
4. Cang J, Feldheim DA. Developmental mechanisms of topographic map formation and alignment. *Annu Rev Neurosci*. 2013;36:51–77.
5. Dickson BJ. Molecular mechanisms of axon guidance. *Science*. 2002;298:1959–1964.
6. Berghuis P, Rajnicek AM, Morozov YM, et al. Hardwiring the brain: endocannabinoids shape neuronal connectivity. *Science*. 2007;316:1212–1216.
7. Berghuis P, Dobszay MB, Wang X, et al. Endocannabinoids regulate interneuron migration and morphogenesis by transactivating the TrkB receptor. *Proc Natl Acad Sci U S A*. 2005;102:19115–19120.
8. Harkany T, Keimpema E, Barabás K, Mulder J. Endocannabinoid functions controlling neuronal specification during brain development. *Mol Cell Endocrinol*. 2008;286(1–2 suppl 1):S84–S90.
9. Harkany T, Mackie K, Doherty P. Wiring and firing neuronal networks: endocannabinoids take center stage. *Curr Opin Neurobiol*. 2008;18:338–345.
10. Watson S, Chambers D, Hobbs C, Doherty P, Graham A. The endocannabinoid receptor, CB1, is required for normal axonal growth and fasciculation. *Mol Cell Neurosci*. 2008;38:89–97.
11. Wu CS, Zhu J, Wager-Miller J, et al. Requirement of cannabinoid CB(1) receptors in cortical pyramidal neurons for appropriate development of corticothalamic and thalamocortical projections. *Eur J Neurosci*. 2010;32:693–706.
12. Argaw A, Duff G, Zabouri N, et al. Concerted action of CB1 cannabinoid receptor and deleted in colorectal cancer in axon guidance. *J Neureosci*. 2011;31:1489–1499.
13. Duff G, Argaw A, Cecyre B, et al. Cannabinoid receptor CB2 modulates axon guidance. *PLoS One*. 2013;8:e70849.
14. Zabouri N, Bouchard JF, Casanova C. Cannabinoid receptor type 1 expression during postnatal development of the rat retina. *J Comp Neurol*. 2011;519:1258–1280.
15. Bouskila J, Burke MW, Zabouri N, Casanova C, Ptito M, Bouchard JF. Expression and localization of the cannabinoid receptor type 1 and the enzyme fatty acid amide hydrolase in the retina of vervet monkeys. *Neuroscience*. 2012;202:117–130.
16. Moldrich G, Wenger T. Localization of the CB1 cannabinoid receptor in the rat brain. An immunohistochemical study. *Peptides*. 2000;21:1735–1742.
17. Grinvald A, Lieke E, Frostig RD, Gilbert CD, Wiesel TN. Functional architecture of cortex revealed by optical imaging of intrinsic signals. *Nature*. 1986;324:361–364.
18. Ridder W III, Nusinowitz S, Heckenlively JR. Causes of cataract development in anesthetized mice. *Exp Eye Res*. 2002;75:365–370.
19. Kalatsky VA, Stryker MP. New paradigm for optical imaging: temporally encoded maps of intrinsic signal. *Neuron*. 2003;38:529–545.
20. Vanni MP, Provost J, Casanova C, Lesage F. Bimodal modulation and continuous stimulation in optical imaging to map direction selectivity. *Neuroimage*. 2010;49:1416–1431.
21. Vanni MP, Murphy TH. Mesoscale transcranial spontaneous activity mapping in GCaMP3 transgenic mice reveals extensive reciprocal connections between areas of somatomotor cortex. *J Neurosci*. 2014;34:15931–15946.
22. Fox MD, Zhang D, Snyder AZ, Raichle ME. The global signal and observed anticorrelated resting state brain networks. *J Neurophysiol*. 2009;101:3270–3283.
23. Cang J, Rentería RC, Kaneko M, Liu X, Copenhagen DR, Stryker MP. Development of precise maps in visual cortex requires patterned spontaneous activity in the retina. *Neuron*. 2005;48:797–809.
24. Cang J, Niell CM, Liu X, Pfeiffenberger C, Feldheim DA, Stryker MP. Selective disruption of one Cartesian axis of cortical maps and receptive fields by deficiency in ephrin-As and structured activity. *Neuron*. 2008;57:511–523.
25. Marshel JH, Garrett ME, Nauhaus I, Callaway EM. Functional specialization of seven mouse visual cortical areas. *Neuron*. 2011;72:1040–1054.
26. Drager UC. Receptive fields of single cells and topography in mouse visual cortex. *J Comp Neurol*. 1975;160:269–290.
27. Gordon JA, Stryker MP. Experience-dependent plasticity of binocular responses in the primary visual cortex of the mouse. *J Neurosci*. 1996;16:3274–3286.
28. Wagor E, Mangini NJ, Pearlman AL. Retinotopic organization of striate and extrastriate visual cortex in the mouse. *J Comp Neurol*. 1980;193:187–202.
29. Albrecht DG, Hamilton DB. Striate cortex of monkey and cat: contrast response function. *J Neurophysiol*. 1982;48:217–237.
30. Sclar G, Maunsell JH, Lennie P. Coding of image contrast in central visual pathways of the macaque monkey. *Vision Res*. 1990;30:1–10.
31. McLaughlin T, O'Leary DD. Molecular gradients and development of retinotopic maps. *Annu Rev Neurosci*. 2005;28:327–355.
32. Young TR, Bourke M, Zhou X, et al. Ten-m2 is required for the generation of binocular visual circuits. *J Neurosci*. 2013;33:12490–12509.
33. Pinar-Sueiro S, Zorrilla Hurtado JÁ, Veiga-Crespo P, Sharma SC, Vecino E. Neuroprotective effects of topical CB1 agonist WIN 55212-2 on retinal ganglion cells after acute rise in intraocular pressure induced ischemia in rat. *Exp Eye Res*. 2013;110:55–58.
34. Rash BG, Grove EA. Area and layer patterning in the developing cerebral cortex. *Curr Opin Neurobiol*. 2006;16:25–34.
35. O'Leary DD, Nakagawa Y. Patterning centers, regulatory genes and extrinsic mechanisms controlling arealization of the neocortex. *Curr Opin Neurobiol*. 2002;12:14–25.
36. Crair MC, Ruthazer ES, Gillespie DC, Stryker MP. Relationship between the ocular dominance and orientation maps in visual cortex of monocularly deprived cats. *Neuron*. 1997;19:307–3418.
37. Hübener M, Shoham D, Grinvald A, Bonhoeffer T. Spatial relationships among three columnar systems in cat area 17. *J Neurosci*. 1997;17:9270–9284.
38. Lowel S, Schmidt KE, Kim DS, et al. The layout of orientation and ocular dominance domains in area 17 of strabismic cats. *Eur J Neurosci*. 1998;10:2629–2643.
39. Grubb MS, Rossi FM, Changeux JP, Thompson ID. Abnormal functional organization in the dorsal lateral geniculate nucleus

Investigative Ophthalmology & Visual Science

of mice lacking the beta 2 subunit of the nicotinic acetylcholine receptor. *Neuron*. 2003;40:1161–1172.

40. Wang L, Rangarajan KV, Lawhn-Heath CA, et al. Direction-specific disruption of subcortical visual behavior and receptive fields in mice lacking the beta2 subunit of nicotinic acetylcholine receptor. *J Neurosci*. 2009;29:12909–12918.
41. Maffei L, Fiorentini A. The visual cortex as a spatial frequency analyser. *Vision Res*. 1973;13:1255–1267.
42. Solomon SG, Peirce JW, Dhruv NT, Lennie P. Profound contrast adaptation early in the visual pathway. *Neuron*. 2004;42:155–162.
43. Cecyre B, Zabouri N, Huppé-Gourgues F, Bouchard JF, Casanova C. Roles of cannabinoid receptors type 1 and 2 on the retinal function of adult mice. *Invest Ophthalmol Vis Sci*. 2013;54:8079–8090.
44. Baccus SA, Meister M. Fast and slow contrast adaptation in retinal circuitry. *Neuron*. 2002;36:909–919.
45. Dasilva MA, Grieve KL, Cudeiro J, Rivadulla C. Endocannabinoid CB1 receptors modulate visual output from the thalamus. *Psychopharmacology (Berl)*. 2012;219:835–845.
46. Boynton GM, Demb JB, Glover GH, Heeger DJ. Neuronal basis of contrast discrimination. *Vision Res*. 1999;39:257–269.
47. Crozier RA, Wang Y, Liu CH, Bear MF. Deprivation-induced synaptic depression by distinct mechanisms in different layers of mouse visual cortex. *Proc Natl Acad Sci U S A*. 2007;104:1383–1388.
48. Jiang B, Huang S, de Pasquale R, et al. The maturation of GABAergic transmission in visual cortex requires endocannabinoid-mediated LTD of inhibitory inputs during a critical period. *Neuron*. 2010;66:248–259.
49. Garkun Y, Maffei A. Cannabinoid-dependent potentiation of inhibition at eye opening in mouse V1. *Front Cell Neurosci*. 2014;8:46.
50. Yoneda T, Kameyama K, Esumi K, Daimyo Y, Watanabe M, Hata Y. Developmental and visual input-dependent regulation of the CB1 cannabinoid receptor in the mouse visual cortex. *PLoS One*. 2013;8:e53082.
51. Nassi JJ, Callaway, EM. Parallel processing strategies of the primate visual system. Nature reviews. *Neuroscience*. 2009;10:360–372.
52. Gao E, DeAngelis GC, Burkhalter A. Parallel input channels to mouse primary visual cortex. *J Neurosci*. 2010;30:5912–5926.
53. Sceniak MP, Ringach DL, Hawken MJ, Shapley R. Contrast's effect on spatial summation by macaque V1 neurons. *Nature Neurosci*. 1999;2:733–739.
54. Sceniak MP, Hawken MJ, Shapley R. Contrast-dependent changes in spatial frequency tuning of macaque V1 neurons: effects of a changing receptive field size. *J Neurophysiol*. 2002;88:1363–1373.
55. Lerner AG, Goodman C, Rudinski D, Bleich A. Benign and time-limited visual disturbances (flashbacks) in recent abstinent high-potency heavy cannabis smokers: a case series study. *Isr J Psychiatry Relat Sci*. 2011;48:25–29.
56. West ME. Cannabis and night vision. *Nature*. 1991;351:703–704.
57. Russo EB, Merzouki A, Mesa JM, Frey KA, Bach PJ. Cannabis improves night vision: a case study of dark adaptometry and scotopic sensitivity in kif smokers of the Rif mountains of northern Morocco. *J Ethnopharmacol*. 2004;93:99–104.
58. Pertwee RG, Howlett AC, Abood ME, et al. International union of basic and clinical pharmacology. LXXIX. Cannabinoid receptors and their ligands: beyond CB(1) and CB(2). *Pharmacol Rev*. 2010;62:588–631.
59. Johnson CA, Casson EJ. Effects of luminance, contrast, and blur on visual acuity. *Optom Vis Sci*. 1995;72:864–869.
60. Dawson WW, Jiménez-Antillon CF, Perez JM, Zeskind JA. Marijuana and vision–after ten years' use in Costa Rica. *Invest Ophthalmol Vis Sci*. 1977;16:689–699.
61. Hirsch J, Curcio CA. The spatial resolution capacity of human foveal retina. *Vision Res*. 1989;29:1095–1101.

Investigative Ophthalmology & Visual Science